Time-Efficient Simulation of Free-Space Optical Communication Systems Under Atmospheric Turbulence, Pointing Error, and Angle-of-Arrival Fluctuations

Mat T. Nguyen, Vuong Mai, *Member, IEEE*, and Hoon Kim, *Senior Member, IEEE*

***Abstract*—Computer simulation is a powerful and convenient tool for the design and performance evaluation of free-space optical (FSO) communication systems. In this article, we present two simulation frameworks that incorporate not only the effects of atmospheric turbulence but also the impact of the angular fluctuations of the transmitter and receiver in FSO systems. In the first framework, the waveform of the optical signal is calculated sequentially from the transmitter to the receiver. Thus, it takes very long to run the simulation numerous times to obtain the statistical performance of the system. This is because the vast majority of simulation time is spent on the split-step beam propagation. In the second framework, we propose to isolate the beam propagation through atmospheric channel from the other effects. We compare the two frameworks in terms of accuracy and simulation time. We show that the second framework reduces the simulation time by more than a factor of 10 without sacrificing the accuracy under various conditions.**

***Index Terms*—Angle of arrival fluctuations, atmospheric turbulence, free-space optical communications, pointing error, simulation study.**

I. Introduction

FREE-SPACE optical (FSO) communications enable high-speed (e.g., >10 Gb/s) wireless transmission without using scarce radio-frequency resources. Thus, they are gaining popularity in various applications such as defense, satellite communications, and wireless fronthaul/backhaul networks.

The performance of FSO communication system is affected by various factors such as the channel characteristics and the alignment of the transmitter and receiver. Atmospheric channel not only attenuates the light intensity through absorption and scattering, but it also distorts the wavefronts of optical signal due to the inhomogeneity of the spatial distribution of refractive index. In particular, the wavefront distortions caused by atmospheric turbulence manifest themselves even on a clear day as scintillation, beam wandering, angle-of-arrival (AoA) fluctuations, and beam spreading. The FSO systems are also highly vulnerable to the alignment of the transmitter and receiver. Highly precise alignment could be a daunting task when the transmitter and receivers are on the move. Angular fluctuations at the transmitter side (caused for example by vibrations) make the pointing errors. On the other hand, the angular fluctuations at the receiver side mainly cause AoA fluctuations. Even fixed point-to-point FSO systems would suffer from the misalignment between the transmitter and receiver due to building sway, dynamic wind loads, and other environmental factors. The misalignment, regardless of its sources, gives rise to a reduction in the received optical power, which in turn, degrades the bit-error ratio (BER) performance of the system.

It is common to utilize the computer simulation for the design and performance evaluation of FSO systems. This is because we can evaluate the system performance under any conditions of atmospheric channel. For example, exceptionally turbulent channel conditions can be readily generated by computer simulation. Also, the simulation study facilitates the statistical analysis of FSO systems in comparison with experimental measurement. The performance of FSO communication system tends to fluctuate over time even under similar strength of atmospheric turbulence. Thus, it is absolutely necessary to obtain the probability density function (PDF) of the received optical power or BER to fully assess the system performance. Numerous cases of turbulent channels generated by computer simulation enable us to obtain those PDFs for comprehensive analysis. Another advantage of utilizing the computer simulation over experiment is that we can isolate a certain effect from others. For example, the impact of misalignment on the system performance could be studied independently of the channel effects by making the channel ideal in the simulation. By contrast, theoretical analysis is a powerful method that offers immediate estimations of the system performance over a range of channel conditions [1], [2], [3]. However, there exist some discrepancies between theoretical and experimental results due to many assumptions and approximations adopted in the development of theoretical analysis [4]. Simulation results, on the other hand, exhibit much better agreement with experiment results than theoretical analyses [5].

Manuscript received 1 August 2023; revised 5 September 2023; accepted 2 October 2023. Date of publication 5 October 2023; date of current version 25 October 2023. This work was supported by the National Research Foundation of Korea through Space HR&D Center Funded by the Ministry of Science and ICT under Grant 2022M1A3C2069728. *(Corresponding author: Hoon Kim.)*

Mat T. Nguyen and Hoon Kim are with the School of Electrical Engineering, Korea Advanced Institute of Science and Technology, Daejeon 34141, South Korea (e-mail: hoonkim@kaist.ac.kr).

Vuong Mai is with the Faculty of Engineering and Informatics, University of Bradford, BD7 1DP Bradford, U.K.

Digital Object Identifier 10.1109/JPHOT.2023.3322159

For the calculation of wave propagation over atmospheric turbulent channel, it is common to solve the stochastic wave equation using the split-step method [6]. In this method, thin phase screens are placed evenly along the transmission path to represent inhomogeneous spatial distribution of refractive index. It is free-space propagation between the phase screens. Commonly, the free-space propagation of optical beam is solved in the spatial frequency domain, whereas the beam propagation through the phase screen is calculated in the space domain [7]. The simulation results obtained by using the phase screens agree with experimental ones [8]. There were a lot of simulation studies to analyze the performance of FSO systems under atmospheric turbulence [9], [10], [11]. Also, various atmospheric turbulence mitigation techniques have been proposed and evaluated through computer simulation [12]. However, these simulation studies focus mainly on the impact of atmospheric turbulence on the system performance. They do not include the effects of misalignment caused by angular fluctuations of the transmitter and receiver.

In this article, we present two simulation frameworks for FSO communication systems that incorporate not only the effects of atmospheric turbulence but also the impact of the angular fluctuations of the transmitter and receiver. To the best of our knowledge, this is the first systematic study on the simulation of FSO communication systems that the effects of pointing errors and AoA fluctuations are amalgamated with the split-step beam propagation through atmospheric channel.

In the first simulation framework (hereafter referred to as Simulation 1), the waveform of the optical signal is calculated sequentially from the transmitter to the receiver. The optical signal is first generated at the transmitter and sent to the channel. The pointing error induced by transmitter vibration is generated in a random manner. Then, the optical beam propagation through atmospheric turbulent channel is simulated by solving the stochastic wave equation. At the receiver, we include the effects of AoA fluctuations in the simulation by tilting the propagation direction of optical signal with respect to the optical axis of the receiver. After detecting the received optical signal, we demodulate the signal and then finally measure the BER performance. In Simulation 1, this entire procedure needs to be repeated a few tens of thousand times to obtain the PDFs of the received optical power and BER. Due to the large number of simulation runs, however, it takes very long (e.g., a couple of weeks) to obtain the PDFs.

In order to reduce the total simulation time dramatically, we propose a novel simulation framework (hereafter referred to as Simulation 2) in this article. The key idea is to isolate the beam propagation through atmospheric channel from the other effects. We realize that the vast majority of simulation time is spent on the beam propagation. Thus, by solving the beam propagation independently of the other effects and then combining the optical field after propagation with the other effects (uncorrelated with beam propagation), we can reduce the number of simulations for beam propagation significantly, and thus the total simulation time. We show that the results of Simulation 2 agree very well with those of Simulation 1, but Simulation 2 saves the total simulation time by more than a factor of 10.

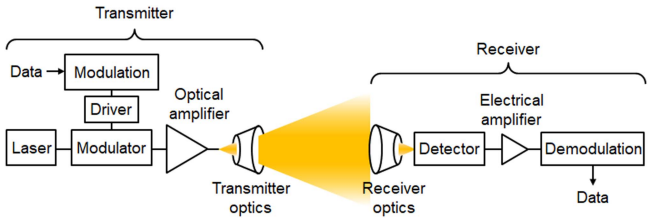

Fig. 1. Schematic diagram of FSO communication system.

The rest of this article is organized as follows. Presented in Section II are the simulation methodology and the proposed simulation frameworks. In Section III, we implement the simulations based on the two frameworks and then compare them in terms of accuracy and simulation time. Finally, we conclude the article in Section IV.

II. Simulation Methodology

Fig. 1 illustrates the schematic diagram of an FSO communication system. At the transmitter, electrical data are fed to the optical modulator for electrical-to-optical conversion. After amplification, the optical signal is emitted to free-space channel via the transmitter optics. At the receiver side, a receiver optics is used to capture the optical signal and couple it to the detector. The detected signal is demodulated and then we evaluate the BER performance.

In the following subsections, we explain the computer simulation of atmospheric channel, pointing errors, AoA fluctuations, and optical elements. Then, the methodology for the two simulation frameworks is presented.

A. Simulation of Atmospheric Turbulence

Atmospheric turbulence pertains to fluctuations in refractive index randomly distributed over space and varying over time. Therefore, atmospheric turbulence can be modeled as a random process. There are some commonly used power spectrum models for refractive-index fluctuations including the Kolmogorov power-law spectrum, Tatarskii spectrum, von Karman spectrum, modified von Karman spectrum, and Hill spectrum [13]. The simplest and practical model that includes effects of inner and outer scales of turbulence is the modified von Karman model. The three-dimensional spatial power spectrum of refractive index fluctuations of the modified von Karman model is defined as follows

$$\Phi_n(\kappa) = \frac{0.033\, C_n^2 \exp\left(-\frac{\kappa^2}{\kappa_m^2}\right)}{\left(\kappa^2 + \kappa_0^2\right)^{11/6}} \quad 0 \le \kappa < \infty \tag{1}$$

Here, $\kappa = \sqrt{\kappa_x^2 + \kappa_y^2 + \kappa_z^2}$ is the three-dimensional spatial wavenumber and C_n^2 represents the refractive index structure constant. Also, $\kappa_m = 5.92/l_0$ and $\kappa_0 = 2\pi/L_0$ are the scalar spatial frequencies, where l_0 and L_0 are the inner and outer scales of turbulence, respectively. For mathematical simplification in computer simulation, a commonly used technique is to treat turbulence as a finite number of discrete layers. Each layer can be

represented by a thin phase screen which represents a turbulent volume of a much greater thickness. There are a couple of ways of generating the phase screen [14], [15]. Among them, the fast Fourier transform (FFT)-based method is widely utilized due to its simplicity and fast computation time. However, this method might suffer from the under-sampling of the low and high spatial frequency components. This problem can be resolved by using the sub-harmonic method and the covariance-matrix method [15], [16]. It should be noted that although atmospheric turbulence varies over time, due to slow temporal characteristics of turbulence (typically >1 ms of time scale) relative to the symbol duration, the atmospheric turbulent channel can be regarded as quasi-static. Thus, static phase screens can be used to represent atmospheric turbulence.

Throughout this article, we assume that the optical signal propagates along the positive z-axis ($\kappa_z = 0$) and the plane of phase screen is orthogonal to the direction of propagation. We also utilize the FFT-based method for the generation of phase screens. Then, the phase of the screen is given by [14]

$$\phi\left(x,\ y\right) = \sum_{\kappa_x}\sum_{\kappa_y} h\left(\kappa_x,\ \kappa_y\right) \times \sqrt{F_\phi\left(\kappa_x,\ \kappa_y\right)} e^{i\left(\kappa_x x + \kappa_y y\right)} \Delta\kappa_x \Delta\kappa_y, \quad (2)$$

where $F_\phi(\kappa_x,\ \kappa_y)$ is the two-dimensional power spectrum of refractive index fluctuations and $h(\kappa_x,\ \kappa_y)$ is a zero-mean unit-variance Hermitian complex Gaussian white noise process.

Wave propagation through the atmospheric turbulence channel can be described by the stochastic wave equation. The scalar form of the wave equation under the paraxial approximation is expressed as

$$\left(\frac{\partial^2}{\partial x^2} + \frac{\partial^2}{\partial y^2}\right) E + 2ik\frac{\partial E}{\partial z} + 2k^2 n\left(\boldsymbol{R}\right) E \ = \ 0\,, \quad (3)$$

where E indicates the electric field, k is the wave number, and $n(\boldsymbol{R})$ represents the refractive index fluctuations in the medium at the point in space $\boldsymbol{R}$. This equation can be solved numerically by using the split-step method [6]. In this method, the propagation link is divided into multiple segments, where each segment is composed of free-space beam propagation and a thin phase screen. The wave equation is solved numerically in the simulation sequentially. In the free-space beam propagation, $n(\boldsymbol{R}) = 0$ in (3). Then, the paraxial wave equation can be solved by using the Huygens-Fresnel integral. Thus, the electric field at the observation plane $(z + \Delta z)$ is computed from the previous plane (z) as follows

$$E\left(x,\ y,\ z + \Delta z\right) = \mathcal{F}^{-1}\left[\mathcal{F}\left\{E\left(x,\ y,\ z\right)\right\} \times \exp\left(\frac{\kappa_x^2 + \kappa_y^2}{2k_0} i\Delta z\right)\right], \quad (4)$$

where $\mathcal{F}$ and $\mathcal{F}^{-1}$ are Fourier transform and inverse Fourier transform, respectively. After the free-space beam propagation, the optical beam is sent to a thin phase screen. The electric field after the phase screen can be solved by setting the first term in (3) to zero. Thus, it is expressed by

$$E_+\ \left(x,\ y,\ z\right) = E_-\ \left(x,\ y,\ z\right) \exp\left\{i\phi\left(x,\ y\right)\right\}, \quad (5)$$

where E_+ and E_- are electric fields right after and before the phase screen, respectively. The process of solving the beam propagation through free-space and phase screen is repeated in the next segment until the optical beam reaches the end of the propagation link.

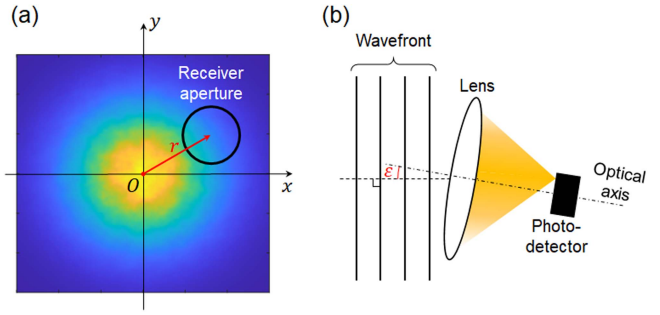

Fig. 2. (a) Optical beam on the receiver aperture plane. Pointing errors induce displacement between the beam's footprint and receiver aperture. (b) Angular displacement of ε between the direction of wavefronts and the optical axis of the receiver induced by AoA fluctuation.

B. Simulation of Pointing Errors

In the FSO system, the transmitter and receiver need to be aligned precisely to the direction of each other. However, the transmitter under mechanical vibrations and/or movement suffers from angular fluctuations of the transmitter, and as a result, pointing errors arise. As illustrated in Fig. 2(a), pointing errors lead to the displacement of optical beam's footprint with respect to the receiver aperture. This displacement in the receiver aperture plane can be expressed as

$$r\ = \sqrt{r_x^2 + r_y^2}, \quad (6)$$

where r_x and r_y are vertical and horizontal displacements of the beam, respectively. Both are modeled as independent, identically distributed zero-mean Gaussian random variables with variance σ_{rx}^2 and σ_{ry}^2, respectively, i.e., $r_x \sim N(0,\ \sigma_{rx}^2)$ and $r_y \sim N(0,\ \sigma_{ry}^2)$. Since only a portion of the beam's footprint is captured by the receiver aperture, the remaining portion falling outside of the receiver aperture is lost. This loss is referred to as geometric loss. Obviously, the geometric loss increases as pointing errors become large. Given the radial displacement of r, the geometric loss (i.e., fraction of optical power collected at the receiver aperture) in a linear scale can be expressed as

$$h_p = \frac{\iint_{\mathcal{A}} I\left(x,\ y\right) dxdy}{\iint_{-\infty}^{\infty} I\left(x,\ y\right) dxdy}, \quad (7)$$

where $I(x,\ y)$ is the intensity of the optical beam at the aperture plane. Also, $\mathcal{A}\ = \ \{(x,\ y) : (x - r_x)^2 + (y - r_y)^2 \le R_a^2\}$ is the aperture function, where R_a is the radius of receiver aperture.

C. Simulation of AoA Fluctuations

AoA fluctuations manifest themselves as the movement of focused optical beam on the detector plane, as illustrated in Fig. 2(b). They degrade the performance of FSO systems by reducing the optical power onto the detector. Angle of arrival, denoted by ε in the figure, is defined by the angular displacement between the direction of the wavefront and the optical axis of the receiver. AoA fluctuations mainly come from the receiver vibration, but atmospheric turbulence and vibrations at the transmitter side also affect AoA fluctuations.

The horizontal and vertical angular displacement, denoted by ε_x and ε_y, respectively, can be modeled as independent, identically distributed zero-mean Gaussian random variables with variance $\sigma^2_{\varepsilon x}$ and $\sigma^2_{\varepsilon y}$, respectively, i.e., $\varepsilon_x \sim N(0,\ \sigma^2_{\varepsilon x})$ and $\varepsilon_y \sim N(0,\ \sigma^2_{\varepsilon y})$ [17]. Thus, the total angular deviation is defined by

$$\varepsilon\ = \sqrt{\varepsilon_x^2 + \varepsilon_y^2} \tag{8}$$

Then, the electric field on the receiver aperture plane in the presence of AoA fluctuation is expressed as

$$E_{AoA}\,(x,\ y,\ z) = E\,(x,\ y,\ z)\exp\left\{-ik\,(x\sin\varepsilon_x + y\sin\varepsilon_y)\right\}, \tag{9}$$

where $E(x,\ y,\ z)$ is the electric field on the receiver aperture plane in the absence of AoA fluctuation.

D. Simulation of Optical Elements

The electric field propagating through optical elements such as transmitter and receiver optics can be calculated in the simulation through the angular-spectrum propagation method. In this method, the angular spectrum of the light beam is calculated by taking the Fourier transform of the light field in the spatial domain [6]. Thus, it allows us to represent the beam propagation through a medium by multiplying the angular spectrum of the light beam with a propagation function that describes the effect of the medium on the light beam. For a short propagation distance with one or more optical elements, an effective way to characterize the beam propagation is utilizing the 2×2 matrix known as ABCD ray-transfer matrix. The ABCD ray-transfer matrix provides a simple and powerful method for analyzing and designing optical systems. It allows us to describe the propagation of a beam through a train of optical elements by multiplying successive matrix representations of each optical element, including the one that describes the free-space propagation between optical elements. Thus, the overall ABCD matrix for *N* optical elements can be expressed as [13]

$$\begin{pmatrix} A & B \\ C & D \end{pmatrix} = \begin{pmatrix} A_N & B_N \\ C_N & D_N \end{pmatrix} \begin{pmatrix} A_{N-1} & B_{N-1} \\ C_{N-1} & D_{N-1} \end{pmatrix} \cdots \begin{pmatrix} A_1 & B_1 \\ C_1 & D_1 \end{pmatrix} \tag{10}$$

The field of the optical wave on the detector plane can be deduced from the generalized Huygens-Fresnel integral as follows

$$E_{\text{out}}\,(x_2,\ y_2) = \frac{e^{ikz}}{i\lambda B} \iint_{-\infty}^{\infty} E_{\text{in}}\,(x_1,\ y_1)\, e^{\frac{ik}{2B}\left(Dr_2^2 - 2r_1r_2 + Ar_1^2\right)} \times dx_1 dy_1, \tag{11}$$

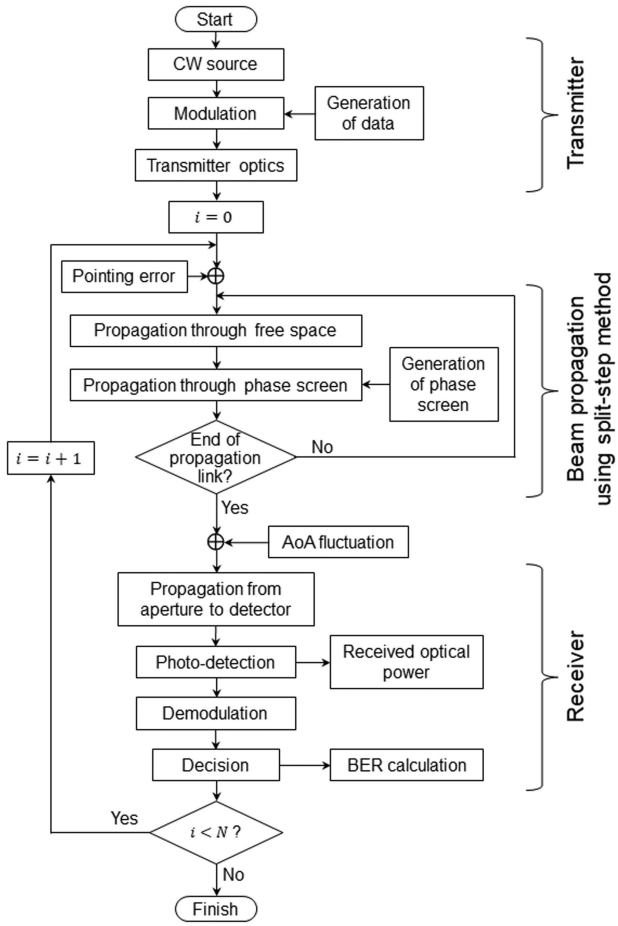

Fig. 3. Flow chart of simulation 1. *N* is the total number of simulations.

where $r_1 = \sqrt{x_1^2 + y_1^2}$ and $r_2 = \sqrt{x_2^2 + y_2^2}$. Also, E_{out} and E_{in} are the output and input electric fields, respectively, and λ indicates the wavelength. By using (11), we can readily solve the wave propagation through multiple optical elements including the effects of AoA fluctuations, rather than solving the wave equation in each optical element.

E. Simulation 1

In this subsection, we present the details of Simulation 1. In this simulation framework, the electric field is calculated sequentially as it propagates over the components in the system. Fig. 3 shows the flow chart of Simulation 1. First, the continuous-wave (CW) electric field is generated to emulate the CW laser. The data are then imposed onto this electric field for optical modulation. For instance, a type of optical modulator such as Mach-Zehnder modulator can be incorporated into the simulation. The beam propagation through the transmitter optics is calculated by using the ABCD ray-transfer matrix, as explained in the previous subsection. Before we employ the split-step beam propagation method, the effects of pointing errors are added to the simulation. As explained in the previous subsection, the pointing errors cause the displacement between the beam's footprint and the receiver aperture. At the receiver side, the effects of AoA fluctuations are included by giving an angular displacement

between the optical axis of the receiver and the direction of the wavefront. After calculating the beam propagation from the receiver optics to the detector using the ray-transfer matrix, we detect the signal, demodulate it, and make decision. The average detected optical power and BER performance are also evaluated at the receiver. In order to assess the system performance statistically, we need to run the simulation numerous times and obtain the PDFs of received optical power and BER. Thus, we repeat the simulation N times. It is interesting to note that there are some random factors in the simulation for given statistical averages. For example, the amounts of pointing error and AoA fluctuation vary in each simulation when these angular displacements follow certain distributions. Random nature of atmospheric turbulence is also included in the phase screen, as shown in (2).

In Simulation 1, a vast majority of simulation time is spent on beam propagation using the split-step method. This is because it involves two-dimensional Fourier and inverse Fourier transforms alternately by the number of phase screens in each simulation. It also demands a considerable amount of simulation time to generate phase screens. To reduce the total simulation time, we propose a novel simulation framework in the next subsection.

F. Simulation 2

In this second simulation framework, we isolate the beam propagation through atmospheric channel from the other effects. The rationale behind the isolation is to reduce the number of simulations for beam propagation through atmospheric channel. The effects of atmospheric turbulence are uncorrelated with the data modulation/demodulation as well as the effects of pointing errors and AoA fluctuations. Thus, it is possible to reduce the simulation number of beam propagation by obtaining the beam propagation independently of the other effects and then combining the optical field after beam propagation with the other effects. Fig. 4 shows the flow chart of Simulation 2. In this proposed simulation framework, we first obtain the BER performance as a function of the received optical power. This is because the characteristics of transmitter and receiver are deterministic and the performance of FSO communication is determined by the received optical power. To obtain the BER versus the received optical power, we make a back-to-back connection between the transmitter and receiver, as illustrated in the flow chart. The BER performance is evaluated as we vary the received optical power. The relationship between the BER and the received optical power will be used to determine the BER performance of the FSO system after we obtain the received optical power in the presence of channel, pointing errors, and AoA fluctuations through simulation. It is worth noting that this relationship is computed only once in the simulation, regardless of the total number of simulations, N.

Next, we calculate the beam propagation through the atmospheric turbulent channel. Since we isolate the effect of beam propagation from the other effects, we simulate the propagation of CW light through atmospheric channel in the absence of pointing errors and AoA fluctuations. Those effects can be readily included after the beam propagation on the receiver's aperture plane, as explained in the previous subsections.

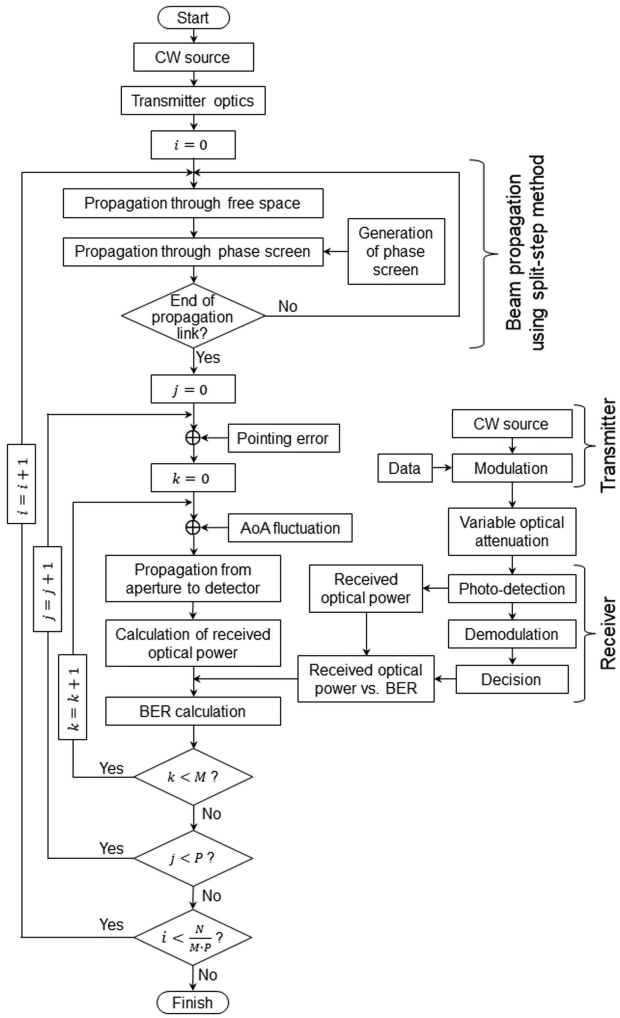

Fig. 4. Flow chart of simulation 2. N, M, and P represent the total number of simulations, the number of realizations for pointing errors, and the number of realizations for AoA fluctuations, respectively.

Since the effects of atmospheric turbulence are uncorrelated with those of pointing errors and AoA fluctuations, we can simulate numerous cases of pointing errors and AoA fluctuations for a single case of beam propagation through the channel. In the flow chart, the numbers of realizations for pointing errors and AoA fluctuations are denoted by P and M, respectively. This approach reduces the number of simulations for beam propagation through the channel dramatically since we need to calculate the split-step beam propagation method only $N/(M \cdot P)$ times, instead of N times in Simulation 1.

It is worth noting that although the effects of atmospheric absorption and scattering are not considered in our simulation frameworks, they can be included simply by attenuating the optical power at the receiver. This is because the effects of atmospheric absorption and scattering are generally estimated from the visibility in a phenomenological manner. Kim's model is one of the most popular ones used to estimate the atmospheric loss per length from visibility [18].

TABLE I
PARAMETERS OF THE SIMULATION

Parameter	Value
Wavelength	1550 nm
Data rate	10 Gb/s
Transmitter beam radius	1 mm
Divergence angle	0.5 mrad
Transmission power	10 dBm
Propagation distance	1000 m
Receiver aperture radius	5 cm
Focal length of receiver lens	5 cm
Detector radius	20 μm
Detector responsivity	0.85 A/W
Multiplication factor	20
k-factor	0.5
APD's dark current	50 nA
Bandwidth of APD	7.5 GHz

III. Simulation Results

In this section, we evaluate the two simulation frameworks in terms of accuracy and simulation time. For this purpose, we carry out the simulations using the two frameworks for a 10-Gb/s horizontal FSO communication system depicted in Fig. 1. Table I summarizes the key parameters employed in the simulation. We utilize the on-off keying modulation format and the direct-detection scheme. Other modulation formats and detection schemes could be readily incorporated in the simulation. A Gaussian optical beam having a radius of 1 mm is transmitted over a 1-km atmospheric turbulent channel. The receiver optics is composed of a lens having a 5-cm radius. We utilize an avalanche photodiode (APD) having a multiplication factor of 20. This value of multiplication factor is optimized for the target BER of 3.8×10^{-3}.

For the generation of phase screens, we utilize the modified von Karman model, as formulated in (1). The inner and outer scales of turbulence are set to be 5 mm and 0.5 m, respectively. The size of phase screen is 4096 × 4096. It is important that the phase distribution of a phase screen should adequately represent the actual phase [19]. This can be assured when the phase screen size $A > 5L_0$ and the grid spacing $\Delta x < l_0/3$. Because the number of phase screens directly affects both the system performance and the simulation time, the required number of phase screens needs to be optimized. We assume that very weak intensity fluctuations are produced over the inter-screen distance Δz, i.e., $\sigma_I^2(\Delta z) < 0.1$ [20]. Thus, the number of phase screens can be estimated from $N_{PS} > 10\sigma_I^2(L)$, where N_{PS} is the number of phase screens and $\sigma_I^2(L)$ is the scintillation index on the receiver aperture plane after transmission distance of *L*.

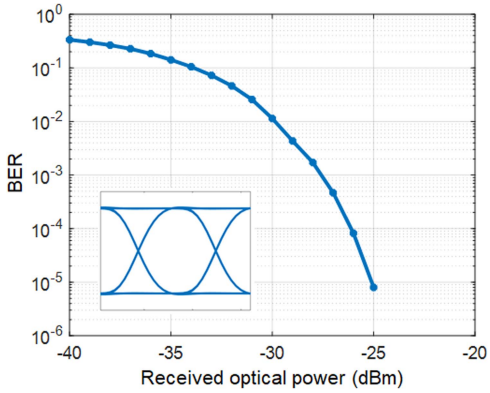

Fig. 5. BER curve obtained by connecting the transmitter and receiver back to back. The inset shows the eye diagram of the optical signal at the output of the transmitter.

The pointing errors and AoA fluctuations are generated randomly and independently for given standard deviations. They follow two-dimensional Gaussian distributions, which are observed in some experiments [21], [22].

We first obtain the transceiver characteristics by measuring the BER performance with respect to the received optical power for the back-to-back link. Fig. 5 shows the result. In this measurement, we employ 10^7 bits. The inset of this figure also shows the eye diagram of the optical signal at the output of the transmitter. The receiver sensitivity (@BER = 3.8×10^{-3}) is measured to be -28.8 dBm. The results of Fig. 5 are used to calculated the BER performance from the received optical power in Simulation 2.

Next, we observe the beam's intensity profile on the receiver aperture plane and the detector plane in the presence of atmospheric turbulence, pointing error, and AoA fluctuations. Fig. 6 shows exemplary beam profiles. Fig. 6(a) shows the beam intensity profile on the receiver aperture plane after transmission over moderate turbulent channel ($C_n^2 = 10^{-14}\ m^{-2/3}$) of 1 km. The size of beam's footprint on the aperture plane is about 1 meter (= 0.5 mrad × 1 km) in diameter. The red circle indicates the receiver aperture. Scintillation is clearly observed in the profile. Also, the figure exhibits the impact of pointing error which induces the displacement of beam's footprint by ∼0.1 m from the receiver aperture. Fig. 6(b) shows the beam profile on the detector plane. The detector (i.e., APD) is indicated by the white circle. Due to the AoA fluctuation of 0.1 mrad, the figure shows the displacement of focused beam from the center of the detector. As another example, we show the intensity profile of the beam on the receiver aperture plane in Fig. 6(c) when the turbulence is strong, i.e., $C_n^2 = 5 \times 10^{-13}\ m^{-2/3}$. Compared to Fig. 6(a), the optical beam suffers more from scintillation. Thus, a tiny portion of the optical beam is collected by the receiver aperture. Also, the optical beam focused by the receiver lens is dispersed in space on the detector plane, as shown in Fig. 6(d).

Fig. 7 shows the histograms of the received optical power and BER performance for the two simulation frameworks when the standard deviations of angular fluctuations of both transmitter and receiver are both 0.15 mrad. Total number of simulations, *N*, is 27000. Due to the large average optical power received at the

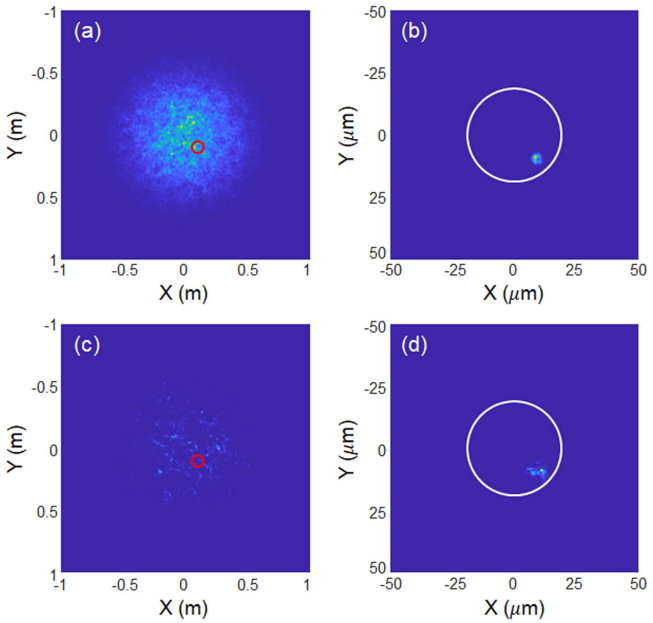

Fig. 6. Beam intensity profiles (a) at the receiver aperture plane and (b) detector plane for $C_n^2 = 10^{-14}\ m^{-2/3}$. Beam intensity profiles (c) at the receiver aperture plane and (d) detector plane for $C_n^2 = 5 \times 10^{-13}\ m^{-2/3}$. The angular displacement at both transmitter and receiver are 0.1 mrad. Red circle represents the receiver aperture, and the white circle represents the APD.

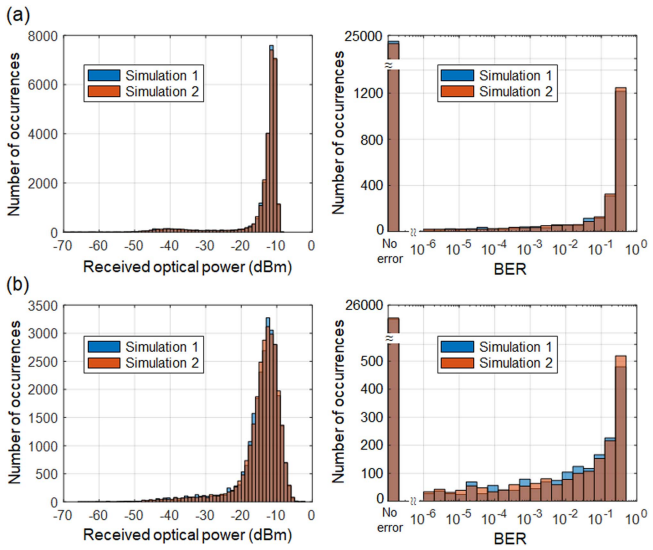

Fig. 7. Histograms of received optical power and BER when the standard deviations transmitter and receiver angular displacement both are 0.15 mrad. (a) $C_n^2 = 10^{-14}\ m^{-2/3}$ (b) $C_n^2 = 5 \times 10^{-13}\ m^{-2/3}$.

receiver (i.e., about −15 dBm), we have error-free transmission in the majority of cases, which are indicated by a large bar on the left side of the BER histograms. In some rare cases, however, the received optical power becomes lower than −40 dBm, and thus we also have poor BER performance. The figure clearly shows that the simulation results of the two frameworks agree very well with each other in both the received optical power and BER performance. Actually, the root-mean-square error between the two histograms under the strong turbulence ($C_n{}^2 = 5 \times 10^{-13}$ m$^{-2/3}$) are calculated to be 1.9×10^{-3} and 6.7×10^{-4}, respectively. Thus, we can say that the histograms obtained from two simulation frameworks exhibit very similar results in terms of the received optical power and BER performance [23].

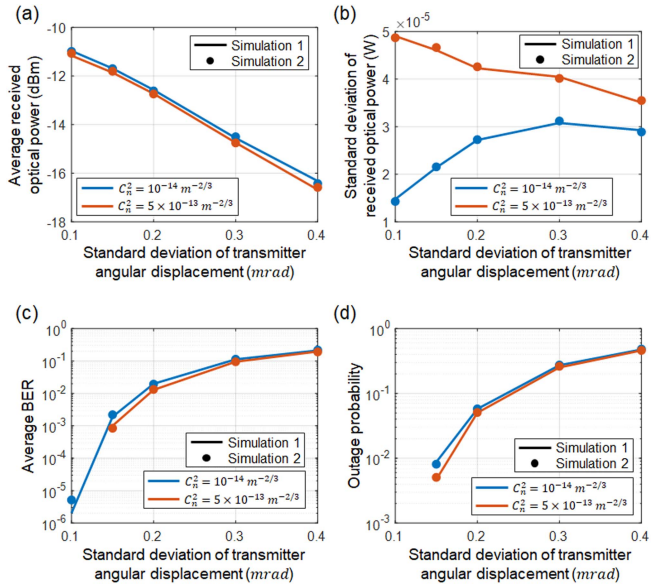

Fig. 8. System performance comparison between two simulations for various amounts of pointing errors. Total number of simulations is 27000. Target BER is 3.8×10^{-3}.

We also compare the results of the two simulation frameworks for various amounts of pointing errors and AoA fluctuations. Fig. 8 shows the average received optical power, standard deviation of received optical power, average BER, and outage probability obtained from the two simulation frameworks as a function of the amount of pointing errors. The outage probability is defined by the probability of having BERs worse than the target BER of 3.8×10^{-3}. The total number of simulations, N, is 27000. For Simulation 2, P and M are both 30. These numbers are selected to make the number of realizations for each effect identical (i.e., $27000^{1/3}$). The figures clearly show that the results of Simulation 2 agree very well with those of Simulation 1 for the two turbulent conditions. It is interesting to note that the average BER performance of FSO system under the strong turbulence ($C_n{}^2 = 5 \times 10^{-13}$ m$^{-2/3}$) is slightly better than that under the moderate turbulence ($C_n{}^2 = 10^{-14}$ m$^{-2/3}$). This is indeed possible since the average optical power under the moderate turbulence is slightly higher than that under the strong turbulence. However, the standard deviation of received optical power under the strong turbulence is larger than that under the moderate turbulence, as evidenced by Fig. 8(b). The histograms illustrated in Fig. 7 also clearly show that the variances of both received optical power and BER for the strong turbulence are much larger than those for the moderate turbulence.

Fig. 9 shows the comparison between the two simulation frameworks when we vary the amount of AoA fluctuations from 0.1 to 0.4 mrad. The figures also show that both frameworks exhibit very similar results in terms of the average received optical power, the standard deviation of the received optical power, average BER, and outage probability.

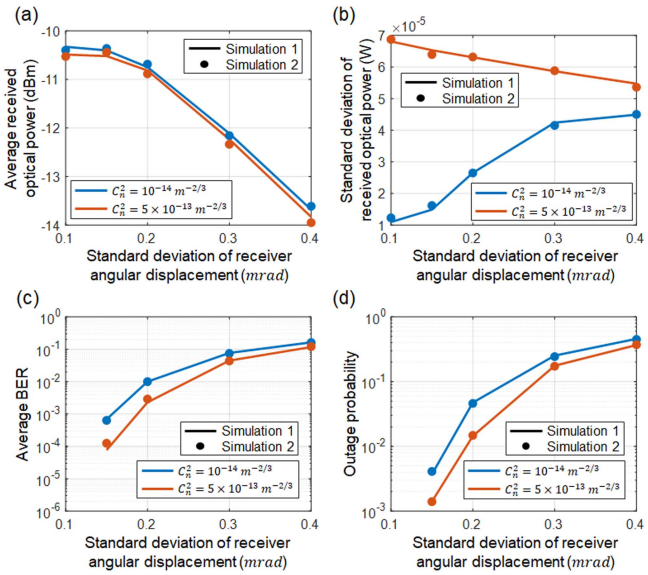

Fig. 9. The system performance comparison between two simulation models for various amounts of AoA fluctuations. Total number of simulations is 27000. Target BER is 3.8×10^{-3}.

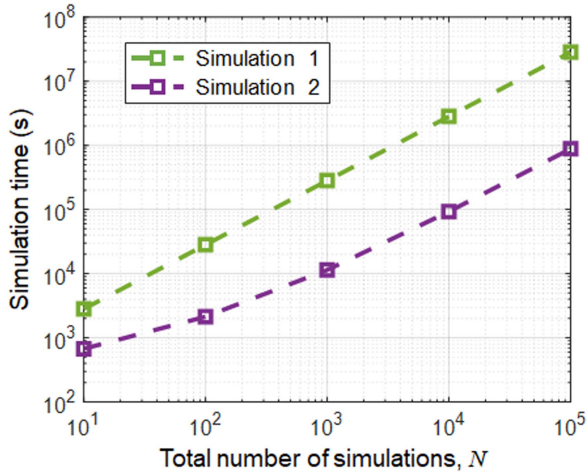

Fig. 10. Total simulation time measured by using a personal computer versus the total number of simulations, N, under strong turbulence ($C_n^2 = 5 \times 10^{-13}\ m^{-2/3}$). The standard deviations of angular fluctuation at both transmitter and receiver are 0.1 mrad.

Finally, we compare the simulation time of the two frameworks. We run both simulations on a personal computer (PC) having Intel Core i7-8700K processor at a maximum clock speed of 3.7 GHz. Fig. 10 shows the simulation time as a function of the total number of simulations under strong turbulence of $C_n{}^2 = 5 \times 10^{-13}$ m$^{-2/3}$. The standard deviations of pointing errors and AoA fluctuations are both 0.1 mrad. The results clearly show that Simulation 2 saves the simulation time roughly by a factor of 30. For example, when the total number of simulations is 10^4, it takes 25.8 hours for Simulation 2, but 32.6 days are required for Simulation 1. This is because Simulation 2 reduces the number of simulations for split-step beam propagation by a factor of $M \cdot P$.

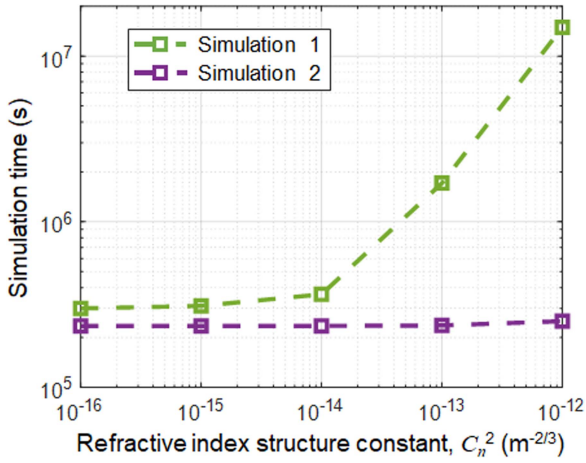

Fig. 11. Simulation time versus the refractive index structure constant. The total number of simulations is 27000.

Fig. 11 shows the simulation time measured by using the PC when we vary the strength of turbulence indicated by the refractive index structure constant. The total number of simulations is 27000. When the turbulence is weak, the required number of segments in the simulation of beam propagation through the atmospheric channel is small [20]. Thus, it takes a short time to simulate the split-step beam propagation. As the turbulence gets stronger, however, the computation of split-step beam propagation becomes heavy, and consequently the simulation time of Simulation 1 increases considerably. Thus, this figure clearly confirms that Simulation 2 saves the simulation time by reducing the number of simulations required for the split-step beam propagation. It also shows that the benefits of Simulation 2 are noticeable when the transmission length is long and/or the turbulence is strong.

IV. Conclusion

We have presented the simulation frameworks for FSO communication systems which incorporate not only the beam propagation through atmospheric turbulent channel but also the effects of the angular fluctuations of the transmitter and receiver. Since the majority of simulation time is spent on the split-step beam propagation over atmospheric channel when the simulations are run numerous times, we can reduce the total simulation time dramatically by isolating the beam propagation from other effects. For this purpose, we generate numerous cases of pointing errors and angle-of-arrival fluctuations independently of the split-step beam propagation. Also, the BER performance as a function of the received optical power is obtained by making the back-to-back connection between the transmitter and receiver in the simulation. In the proposed simulation framework, the received optical powers in the presence of channel, pointing errors, and angle-of-arrival fluctuations are calculated for numerous combinations of those system impairments. Then, the BER performance can be evaluated from the BER versus received optical power. Our simulation study shows that the proposed simulation framework reduces the total simulation time significantly without loss of accuracy. Therefore, we believe that

the proposed simulation framework would be useful especially when we evaluate the performance of FSO communication systems in a statistical manner.

REFERENCES

[1] M. R. Bhatnagar and Z. Ghassemlooy, "Performance analysis of gamma-gamma fading FSO MIMO links with pointing errors," *J. Lightw. Technol.*, vol. 34, no. 9, pp. 2158–2169, May 2016.

[2] Y. Ata and M.-S. Alouini, "Performance of integrated ground-air-space FSO links over various turbulent environments," *IEEE Photon. J.*, vol. 14, no. 6, Dec. 2022, Ar. no. 7358916.

[3] H. S. Khallaf, K. Kato, E. M. Mohamed, S. M. Sait, H. Yanikomeroglu, and M. Uysal, "Composite fading model for aerial MIMO FSO links in the presence of atmospheric turbulence and pointing errors," *IEEE Wireless Commun. Lett.*, vol. 10, no. 6, pp. 1295–1299, Jun. 2021.

[4] W. Moon and H. Kim, "Standard deviation of fiber-coupling efficiency for free-space optical communication through atmospheric turbulence," *IEEE Photon. J.*, vol. 15, no. 3, Jun. 2023, Art. no. 7302507.

[5] S. M. Flatte and G. Y. Wang, "Irradiance variance of optical waves through atmospheric turbulence by numerical simulation and comparison with experiment," *J. Opt. Soc. Amer. A*, vol. 10, no. 11, pp. 2363–2370, 1993.

[6] J. D. Schmidt, *Numerical Simulation of Optical Wave Propagation With Examples in MATLAB*. Bellingham, WA, USA: SPIE, 2010.

[7] S. S. Chesnokov et al., "Numerical/optical simulation of laser beam propagation through atmospheric turbulence," DTIC Document, Tech. Rep. ADA311320, 1995.

[8] K. A. Mudge et al., "Scintillation index of the free space optical channel: Phase screen modelling and experimental results," in *Proc. Int. Conf. Space Opt. Syst. Appl.*, 2011, pp. 403–409.

[9] R. Frehlich, "Simulation of laser propagation in a turbulent atmosphere," *Appl. Opt.*, vol. 39, pp. 393–397, 2000.

[10] Z. Chen et al., "Precision analysis of turbulence phase screens and their influence on the simulation of Gaussian beam propagation in turbulent atmosphere," *Appl. Opt.*, vol. 59, no. 12, pp. 3726–3735, 2020.

[11] D. A. Paulson et al., "Randomized spectral sampling for efficient simulation of laser propagation through optical turbulence," *J. Opt. Soc. Amer. B*, vol. 36, pp. 3249–3262, 2019.

[12] Prasetiyo, V. Mai, H. Kim, and S. H. Cho, "Mitigation of scintillation effect using spectrum-sliced incoherent light source for free-space optical communication," in *Proc. Opto-Electron. Commun. Conf.*, 2020, pp. 1–3.

[13] L. C. Andrews and R. L. Phillips, *Laser Beam Propagation Through Random Media*. Bellingham, WA, USA: SPIE, 2005.

[14] E. M. Johansson and D. T. Gavel, "Simulation of stellar speckle imaging," *Proc. SPIE*, vol. 2200, pp. 372–383, 1994.

[15] J. Xiang, "Accurate compensation of the low-frequency components for the FFT-based turbulent phase screen," *Opt. Exp.*, vol. 20, pp. 681–687, 2011.

[16] B. J. Herman and L. A. Strugala, "Method for inclusion of low-frequency contributions in numerical representation of atmospheric turbulence," *Proc. SPIE*, vol. 1221, pp. 183–192, 1990.

[17] V. V. Mai and H. Kim, "Beam size optimization and airborne free-space optical communication systems," *IEEE Photon. J.*, vol. 11, no. 2, Apr. 2019, Art. no. 7902213.

[18] I. Kim, B. McArthur, and E. J. Korevaar, "Comparison of laser beam propagation at 785 nm and 1550 nm in fog and haze for optical wireless communications," *Proc. SPIE*, vol. 4214, pp. 26–37, 2001.

[19] D. L. Knepp, "Multiple phase-screen calculation of temporal behavior of stochastic waves," *Proc. IEEE*, vol. 71, no. 6, pp. 722–737, Jun. 1983.

[20] J. M. Martin and S. M. Flatte, "Intensity images and statistics from numerical simulation of wave propagation in 3-D random media," *Appl. Opt.*, vol. 27, no. 11, pp. 2111–2126, 1988.

[21] B. Moision et al., "Demonstration of free-space optical communication for long-range data links between ballons on project loon," *Proc. SPIE*, vol. 10096, pp. 259–272, 2017.

[22] T. V. Phuc et al., "Experimental channel statistics of drone-to-ground retro-reflected FSO links with fine-tracking systems," *IEEE Access*, vol. 9, pp. 137148–137164, 2021.

[23] H. Kotake et al., "Experimental analysis of atmospheric channel model with misalignment fading for GEO satellite-to-ground optical link using 'LUCAS' onboard optical data relay satellite," *Opt. Exp.*, vol. 31, no. 13, pp. 21351–21366, 2023.